IL NUOVO CIMENTO VOL. 106 A, N. 12 Dicembre 1993

On Target Design for Heavy-Ion ICF and Gain Scaling (*).

J. MEYER-TER-VEHN, M. BASKO, R. RAMIS and A. RICKERT
Max-Planck-Institut für Quantenoptik - 8046 Garching, Germany

(ricevuto il 25 Maggio 1993; approvato l'1 Giugno 1993)

Summary. — First, gain scaling for ignition experiments recently published by the Livermore group is interpreted within the isobaric gain model. Secondly, two options for indirect drive of fusion targets with heavy-ion beams are compared, one having localized converter elements and the other using low-Z foam in the hohlraum for conversion. In addition, the new code MULTI2D for two-dimensional radiation hydrodynamics simulation is briefly discussed, and also progress in high-Z opacity calculations; both topics are relevant for future target work.

PACS 28.50.Re – Fusion reactors and thermonuclear power studies.

1. – Introduction.

The next major step envisioned in inertial-fusion research is to achieve ignition and fusion burn at one of the big laser facilities. Concerning target performance, these expectations are based on gain predictions published recently by Lindl *et al.* [1]. It is said in the publication that these results were derived from sophisticated numerical simulations that accurately describe laboratory experiments and experiments by means of underground nuclear explosions and that the degree of hydrodynamic stability was kept invariant in these calculations. But details of the calculations were not fully disclosed. In the first part of this paper, we interpret these results in terms of the isobaric gain model [2]. Following results of Atzeni [3], it is shown that the predicted gain scaling can be reproduced almost quantitatively by keeping the average fuel compression invariant (see fig. 1).

The second topic of this paper deals with fusion targets indirectly driven by heavy-ion beams. Indirect drive is considered to be the only realistic option to achieve the required illumination symmetry with ion beam drivers. Open questions exist as to what is the best hohlraum configuration [4]. Different choices concerning the interaction spots at which the ion beams are stopped and heat the hohlraum imply different choices concerning ion energy, beam current, beam focussing and overall

(*) Paper presented at the International Symposium on Heavy Ion Inertial Fusion, Frascati, May 25-28, 1993.

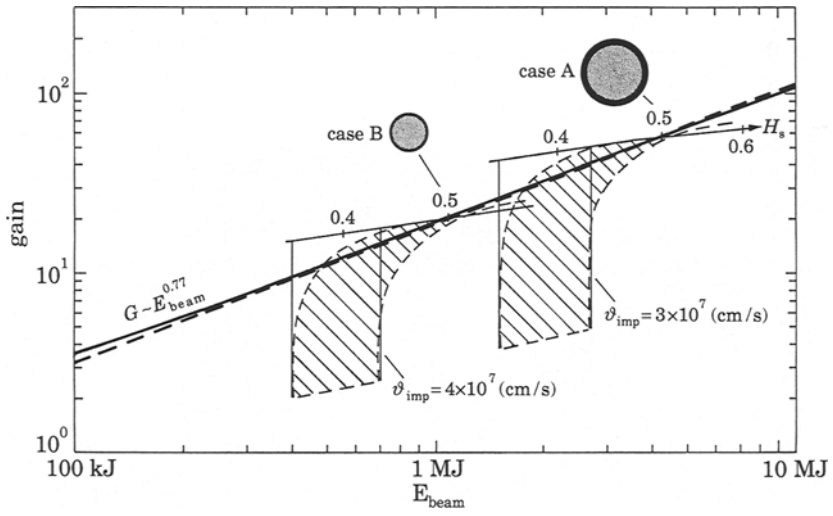

Fig. 1. – Livermore results (dashed lines) compared to model results (solid curves). For details see text. $\eta = 5\%$, $\alpha = 1$.

illumination geometry, and therefore have significant consequences for the driver and reactor design. We have worked out two alternative designs [5, 6]: one has localized converter elements, requiring focussing to small spots ($\simeq 3$ mm), but admitting heavy-ion (*e.g.* Bi) energies up to 10–20 GeV; the other one has the interaction volume spread out over the entire radiation cavity which is filled with low-Z foam. The second design requires less focussing, but admits Bi-ion energies only up to about 6 GeV and, consequently, needs higher beam current.

2. – Gain scaling for ignition experiments.

2·1. *The isobaric gain model.* – The isobaric gain model is described in [2]. It models an isobaric DT ignition configuration with a central ignition sphere (the spark) and a surrounding cold fuel shell, into which burn is propagating after ignition. It allows one to calculate the energy gain

$$G = E_{\text{fusion}}/E_{\text{beam}} = G(E_{\text{beam}};\ p,\ \alpha,\ \eta;\ T_s,\ H_s,\ H_B,\ Q_B), \tag{1}$$

which is the ratio of the fusion energy E_{fusion} released and the absorbed beam energy E_{beam}, as a function of a few parameters. The free parameters are the fuel pressure p at ignition, the coupling efficiency $\eta = E_f/E_{\text{beam}}$, where E_f is the fuel energy at ignition, and the isentrope parameter $\alpha = p/p_{\text{deg}}$ of the cold fuel which is the cold fuel pressure in units of the electron Fermi gas pressure $p_{\text{deg}} = A_0 \rho_c^{5/3}$ with $A_0 = 2.16 \cdot 10^{12}$ in c.g.s. units and the cold fuel density ρ_c. The other parameters are fixed by fusion physics: the ignition temperature $T_s = 5$ keV, the density-radius product $H_s = \rho_s R_s$ of the spark, the burn parameter $H_B = 7\text{g/cm}^2$, controlling the burn efficiency $\Phi = H_f/(H_B + H_f)$, and the specific DT fusion energy release $Q_B = 3.37 \cdot 10^{11}$ J/g; $H_f = \rho_s R_s + \rho_c(R_f - R_s)$ denotes the total fuel ρR where ρ_s is the spark density, ρ_c the cold fuel density, R_s the spark radius, and R_f the total fuel radius.

2'1.1. Gain as a function of ρ_f/ρ_0 and ε_f. In an attempt to introduce symmetry constraints into this model, we select the average fuel compression ρ_f/ρ_0 as a global symmetry measure and compare fuel configurations with the same ρ_f/ρ_0, assuming that they require the same degree of symmetry during implosion. Here, $\rho_f = M_f/(4\pi R_f^3/3)$ is the average fuel density at ignition and $\rho_0 = M_f/(4\pi R_0^2 \Delta R_0)$ the density of the initial cryogenic fuel shell with radius R_0 and thickness ΔR_0. Apparently, the average fuel compression

$$\rho_f/\rho_0 \simeq 3C_f^3/A_0 \tag{2}$$

is uniquely determined by the fuel convergence ratio $C_f = R_0/R_f$ and the aspect ratio $A_0 = R_0/\Delta R_0$ of the initial fuel shell. Both quantities, C_f and $C_f/A_0 = \Delta R_0/R_f$, are restricted by upper bounds due to imperfections in the symmetry of drive and target make, and this limits the values of ρ_f/ρ_0 that can be obtained.

Beside ρ_f we introduce the average internal energy ε_f of the fuel which is related to the implosion velocity v_{imp} by

$$\varepsilon_f = E_f/M_f = \Omega v_{imp}^2 . \tag{3}$$

Here, Ω is a dimensionless mass parameter describing the imploding shell after acceleration. For pure, uniform fuel at zero entropy, one would have $\Omega = 0.5$. However, in real situations $\Omega > 0.5$, since the imploding energy also includes thermal

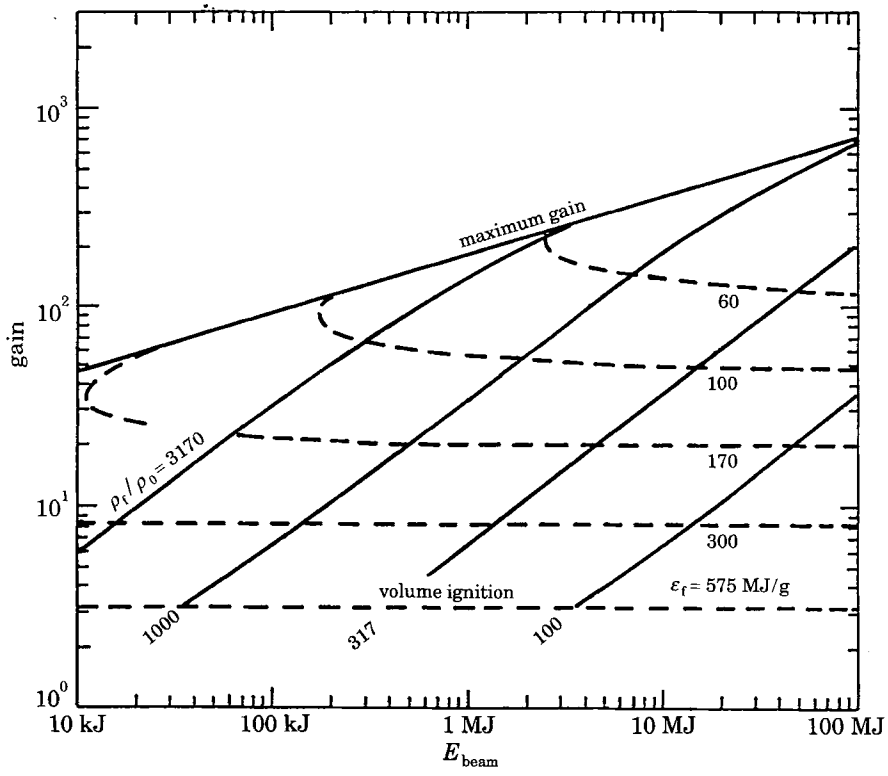

Fig. 2. – Gain curves for fixed ρ_f/ρ_0 (solid lines) and fixed ε_f (dashed lines) with $\eta = 10\%$ and $\alpha = 2$. For details see text.

energy of the fuel. Gain is now studied as a function of ρ_f/ρ_0 and ε_f, replacing E_{beam} and p as independent variables.

Gain curves for $\rho_f/\rho_0 = \text{const}$ (solid lines) and $\varepsilon_f = \text{const}$ (dashed lines) are plotted in fig. 2; the other parameters are $\alpha = 2$ and $\eta = 0.1$. For sufficiently high beam energy, the gain depends on ε_f alone and increases for decreasing ε_f. High-gain regions can be accessed only with low ε_f, corresponding to relatively low implosion velocity. Such implosions involve large fractions of cold fuel with low specific energy and, of course, require spark ignition. On the other hand, volume ignition corresponds to the bottom line with $\varepsilon_f = 575\,\text{MJ/g}$ and low gain. It is noticed that also the gain curves at fixed ρ_f/ρ_0, corresponding to implosions with same fuel convergence, are approximately straight lines.

2·2. *Model fit to Livermore results.* – The Livermore gain prediction for the ignition experiment is shown in fig. 1 as a straight dashed line, scaling with beam energy like $G \propto E_{beam}^{0.77}$. The parameter varying along this line is the implosion velocity v_{imp} (equivalent to ε_f). The gain curve was derived by making a large number of simulation runs and finding the lowest possible v_{imp} consistent with a given driver energy as well as with symmetry constraints and stable ignition. Lindl et al. [1] give the scaling relation

$$E_{beam} \propto \alpha^4 / v_{imp}^5 , \tag{4}$$

where α is the isentrope parameter defined before. The beam energy required for ignition strongly decreases for higher implosion velocity. The two inserts in fig. 1 refer to cases with different implosion velocities, and the shaded areas mark the region of ignition uncertainty; at beam energies a factor 2-3 above the ignition threshold, these uncertainties decrease, and a definite gain is predicted. An energy of 1–2 MJ is required for stable ignition of the case with $v_{imp} = 4 \cdot 10^7\,\text{cm/s}$, which is the reference case for the ignition experiment.

The fit of the isobaric gain model to the Livermore results is shown in fig. 1 by the solid lines. Almost perfect agreement is obtained when keeping the average fuel compression constant at a value $\rho_f/\rho_0 = 1850$, and choosing $\eta = 5\%$, $\alpha = 1$, $H_s = 0.5\,\text{g/cm}^2$. A fit of similar quality could be obtained with somewhat different values of η and H_s after readjusting ρ_f/ρ_0. The low coupling efficiency of $\eta = 5\%$ is chosen here because such values are adequate for indirect drive on which the Livermore results are based. The spark confinement parameter $H_s = 0.5\,\text{g/cm}^2$ is chosen somewhat larger than the threshold value $0.4\,\text{g/cm}^2$ in order to account for an ignition margin. The fitted value $\rho_f/\rho_0 = 1850$ for the compression ratio corresponds to a convergence ratio $C_f \simeq 25$, assuming that $C_f/A_0 = \Delta R_0/R_f = 1$.

The particular cases for $v_{imp} = 3 \cdot 10^7\,\text{cm/s}$ and $v_{imp} = 4 \cdot 10^7\,\text{cm/s}$ are obtained with $\varepsilon_f = \Omega v_{imp}^2$, adjusting the mass parameter to $\Omega = 0.8$. Varying H_s at fixed ρ_f/ρ_0 and fixed ε_f is the way to account for different ignition margins. It produces the lines cutting the general gain curve at $H_s = 0.5\,\text{g/cm}^2$, and the left and right margins of the shaded gain areas are obtained for $H_s = 0.36$ and $H_s = 0.43$, respectively. Of course, the gradual change of the ignition areas from low to high gain is not reproduced in this way, but the remarkable overall agreement indicates that the model is indeed describing essential features of the simulation results.

The gain curve obtained here for fixed ρ_f/ρ_0 depends also on α. Although this dependence is weak, α influences the slope of the gain curve in a distinct way, and the

scaling of the Livermore curve, $G \propto E_{\mathrm{beam}}^{0.77}$, is obtained only with $\alpha = 1$. This may surprise because the isentrope $\alpha = 1$ describes fully degenerate fuel and is practically inconsistent with real target implosions. Actually, the small fit value indicates a shortcoming of the model related to the assumption of uniform pressure. In real target implosions, the fuel pressure at stagnation is not completely uniform, but decreases with radius, and the isobaric model is therefore incorrect in attributing too much compression energy to the cold fuel. This failure becomes particularly severe for cases close to ignition where the cold fuel consists of thin shells at the surface. Within the model framework, the effect of smaller pressure at the outer surface can be partly accounted for by a smaller value of α. More detailed analysis shows that the fitted value $\alpha_{\mathrm{fit}} = 1$ corresponds to an isentrope of $\alpha \simeq 2$.

2·3. *Analytic analysis.* – Close to ignition, a regime exists in which the relations

$$\begin{cases} E_{\mathrm{c}} \ll E_{\mathrm{f}} \simeq E_{\mathrm{s}}\,, \\ M_{\mathrm{s}} \ll M_{\mathrm{f}} \simeq M_{\mathrm{c}} \end{cases} \tag{5}$$

hold at the same time. Although the energy of the cold fuel is still a small fraction of the total fuel energy, the mass of the cold fuel is already a large fraction and exceeds the spark mass. These two inequalities provide the key for describing the low-gain region analytically. It follows from (3.1) that

$$\frac{H_{\mathrm{c}}}{H_{\mathrm{s}}} \simeq \frac{M_{\mathrm{c}}}{4\pi R_{\mathrm{s}}^2 H_{\mathrm{s}}} \simeq \frac{M_{\mathrm{f}}}{4\pi R_{\mathrm{s}}^2 H_{\mathrm{s}}} \simeq \frac{E_{\mathrm{f}}}{4\pi R_{\mathrm{s}}^3 \rho_{\mathrm{s}} \varepsilon_{\mathrm{f}}} \simeq \frac{\varepsilon_{\mathrm{s}}}{3\varepsilon_{\mathrm{f}}}\,, \tag{6}$$

and, taking into account $H_c/H_{\mathrm{s}} = (\rho_{\mathrm{c}} \Delta R_{\mathrm{c}})/(\rho_{\mathrm{s}} R_s)$, $\rho_{\mathrm{c}} \varepsilon_{\mathrm{c}} = \rho_{\mathrm{s}} \varepsilon_{\mathrm{s}} = \rho_{\mathrm{f}} \varepsilon_{\mathrm{f}} = 3p/2$, and $\varepsilon_{\mathrm{c}} = (3/2)(\alpha A_0)^{3/5} p^{2/5}$,

$$\rho_{\mathrm{f}} \simeq 3 \left(\frac{\Delta R_{\mathrm{c}}}{R_{\mathrm{s}}} \right)^{5/2} \left(\frac{2\varepsilon_{\mathrm{f}}}{\alpha A_0} \right)^{3/2}\,, \tag{7}$$

where ΔR_{c} denotes the thickness of the cold fuel layer. Let us first derive the gain at fixed ε_{f}. Approximating the burn efficiency by

$$\Phi = \frac{H_{\mathrm{s}} + H_{\mathrm{c}}}{H_{\mathrm{B}} + H_{\mathrm{s}} + H_{\mathrm{c}}} \simeq 0.1\,(H_{\mathrm{c}}/H_{\mathrm{s}})^{0.6} \tag{8}$$

for $H_{\mathrm{B}}/H_{\mathrm{s}} = 7/0.4$, we find

$$G \simeq \eta Q_{\mathrm{B}} \Phi/\varepsilon_{\mathrm{f}} \propto \varepsilon_{\mathrm{f}}^{-1.6}\,, \tag{9}$$

independent of ρ_{f} in good agreement with the $\varepsilon_{\mathrm{f}} = \mathrm{const}$ curves in fig. 2.

Let us now understand how $E_{\mathrm{f}} = \eta E_{\mathrm{beam}}$ depends on ε_{f} and ρ_{f}. Starting from the identity

$$E_{\mathrm{f}} = E_{\mathrm{s}} \left(\frac{1 - (E_{\mathrm{c}}/E_{\mathrm{s}})(M_{\mathrm{s}}/M_{\mathrm{c}})}{1 - (E_{\mathrm{c}}/E_{\mathrm{f}})(M_{\mathrm{f}}/M_{\mathrm{c}})} \right), \tag{10}$$

we neglect the term $(E_{\mathrm{c}}/E_{\mathrm{s}})(M_{\mathrm{s}}/M_{\mathrm{c}})$ in the numerator, expand the denominator, and

find the leading-order terms

$$E_f \propto \frac{1}{\rho_f^2 \varepsilon_f^2}\left(1 + \left(\frac{3/2\,\alpha A_0 \rho_f^{2/3}}{\varepsilon_f}\right)^{0.6} \pm \ldots\right). \tag{11}$$

Recalling that $\varepsilon_f \propto v_{imp}^2$, we find for fixed ρ_f and α that the E_{beam} scaling varies between $E_{beam} = E_f/\eta \propto v_{imp}^{-4.0} \ldots v_{imp}^{-5.2}$. Taking $E_{beam} \propto v_{imp}^{-4.6}$ as an average and combining it with eq. (8), we find in addition $G \propto E_{beam}^{0.70}$. These scalings are in fair agreement with the Livermore results $E_{beam} \propto 1/v_{imp}^5$ and $G \propto E_{beam}^{0.77}$. They describe the gain at fixed ρ_f and α, and due to relation (6), a change of the fuel aspect ratio $R_s/\Delta R_c \propto v_{imp}^{6/5}$ along the gain curve is implied.

Now changing α at fixed v_{imp}, it is assumed that the configurations along this optimal gain curve are only geometrically scaled, *i.e.* the proportions $R_s : \Delta R_c : R_f$, $\rho_s : \rho_c : \rho_f$, and $\varepsilon_s : \varepsilon_c : \varepsilon_f$ stay invariant and therefore refer to the same degree of stability. This leads to $\rho_f \propto \alpha^{-3/2}$ thanks to eq. (6) and to $E_{beam} \propto \alpha^3$ after insertion into eq. (10). In comparison, the Livermore result is $E_{beam} \propto \alpha^4$.

In conclusion, the isobaric gain model allows one to reproduce the Livermore ignition predictions in much detail when constraining ρ_f and ε_f.

3. – Two options for indirect drive with heavy-ion beams.

The concept of indirect drive is to drive the capsule implosion with thermal X-rays generated by dense high-Z plasma that is hydrodynamically separated from the capsule. In this way, a highly spherical illumination of the capsule can be achieved, even though the incoming beams have low symmetry. Symmetrization is enhanced by placing the capsule inside a cavity which is heated by the beam at some interaction spots.

A major problem inherent in indirect drive is low coupling efficiency. A significant part of beam energy is lost in the process of X-ray conversion and X-ray confinement in the hohlraum. The hohlraum has to be heated to temperatures of $T =$ $= 200$–300 eV to obtain Stefan-Boltzmann fluxes $S = \sigma T^4$ of up to $10^{15}\,\mathrm{W/cm^2}$, as required for successful target implosions. Since plasma specific energies come to several $10^7\,\mathrm{J/g}$ at such temperatures, only small amounts of material can be used for beam conversion and radiation confinement, at most a few 100 mg.

For heavy-ion beam fusion, this sets stringent limits on ranges and energies of beam ions which have to be stopped. One has essentially two choices: 1) either compact cylindrical converter elements with small cross-section allowing for ion ranges of 300–$500\,\mathrm{mg/cm^2}$, however at the price of sharp focussing and pointing of the beams, or 2) low-density stopping material (foams) filling larger regions of the cavity volume and thereby relaxing focussing requirements, however restricting ion ranges to less than $100\,\mathrm{mg/cm^2}$. Examples for both options are now discussed.

3·1. *Hohlraum target with localized converters.* – The hohlraum target with two cylindrical converter elements and target illumination from opposite sides was investigated by Murakami and Meyer-ter-Vehn [5]. A study on converter performance was published separately [7], showing that ion-beam/X-ray conversion efficiencies of $\eta_{con} = 70$–90% can be obtained provided deposition powers are above $10^{16}\,\mathrm{W/g}$. The total efficiency for coupling beam energy into fuel energy at ignition is given by $\eta_c = \eta_{con}\,\eta_{trans}\,\eta_{hyd}$ and involves also the efficiency of energy transfer in the

hohlraum η_{trans} and the hydrodynamic efficiency η_{hyd} of target implosion. For transfer, $\eta_{\text{trans}} \simeq 33\%$ was found, taking gold for the outer casing and carbon for the inner capsule ablator with an area ratio 10 of outer to inner surface; this is a high loss. On the other hand, $\eta_{\text{hyd}} \simeq 18$–$20\%$ was found for radiatively driven implosions, much higher than for directly driven ablation with lasers or ion beams. This leads to an expected total coupling efficiency of $\eta_c \simeq 5\%$ which is sufficient for high-gain targets.

The symmetry aspects of such target configurations were investigated recently in different publications [5, 8, 9]. The result is that two-sided illumination heats the polar regions of the capsule too strongly and that six converter elements, symmetrically distributed in the hohlraum, are needed to achieve the required 1–2% irradiation symmetry. Of course, adding converter elements makes target illumination in a fusion reactor more complex. Two-sided illumination would be attractive, and a way to save this option may be to use additional screening of the converters. This could be done by placing tiny amounts of opaque material between converter and capsule, may be supported by very low-density foam filling the hohlraum. Such options still need to be worked out.

3·2. *Hotraum target design.* – Another alternative is to avoid localized conversion at all and to spread beam energy deposition all over the outer regions of a cavity filled with low-density foam. Such a target is shown schematically in fig. 3, indicating also the incoming beams and the boundary (dotted line) of the deposition volume. The beam configuration illuminating this target is illustrated in fig. 4. It consists of two arrays of individual beams, 10 from above and 10 from below like in the HIBALL reactor study. Analysing deviations from spherical symmetry in terms of multipoles, one finds that the $l = 2$ mode can be eliminated by choosing the angle of incidence $\alpha_0 = 36°$ (first derived in [10]) and the $l = 4$ mode by choosing proper lateral beam profiles. The higher multipoles are smoothed by radiative transport in the cavity [11]. The symmetry aspects are described in [12], and a full 1D analysis is given in [6]. Here, we focus on two outstanding aspects in the dynamics of this targets.

First, the hohlraum is not «hohl» (german word for «empty»), but is filled with

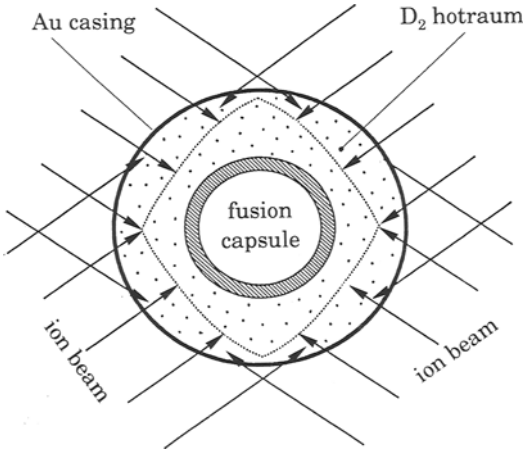

Fig. 3. – Hotraum target configuration. The space between outer gold casing and inner fusion capsule (shaded ring) is filled with low-density low-Z material; the ion beams coming in from different sides penetrate up to the dotted line. For more details see text.

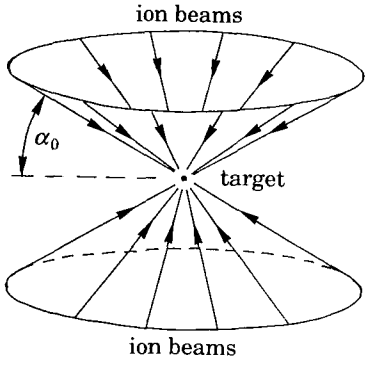

Fig. 4. – Configuration of beams illuminating the hotraum target.

matter which becomes an optically thin plasma after a short ionization phase. We therefore named it «hotraum». Due to this matter fill, energy transport from the deposition region to the fusion capsule is not only by radiative transfer, but also by hydrodynamics, as seen in the flow diagram in fig. 5. This is potentially dangerous because the hydrodynamic waves transport the asymmetric patterns of beam deposition toward the capsule and can even enhance them. In fig. 5, it is assumed that the ion beam penetrates the outer gold shell and is stopped in the hotraum at a radius of 4 mm. A shock is seen running inwards starting from the heated region. A radiation wave (not visible in fig. 5) is passing the inner part of the hotraum much faster (in less than 1 ns), and radiatively driven ablation of the fusion capsule is seen to set in at about 2 ns. An interesting phenomenon is now observed to occur. Apparently, the outward flow of ablated material is strong enough for the parameters chosen here (750 TW, 10 MJ box-shaped beam pulse) to prevent the incoming deposition shock from hitting the capsule shell. Actually, the ablating flow is supersonic insulating the inner implosion dynamics from the asymmetrically incoming fronts of the outer hydrodynamics. This regime is reached only when the driving power exceeds a critical value. We consider the existence of such a regime an important result.

A second crucial aspect concerns the hydrodynamic efficiency η_{hyd} of tamped, radiatively driven ablation in the hotraum; η_{hyd} is defined as fuel energy at ignition divided by the total energy transfered to the capsule. Surprisingly large values of $\eta_{\mathrm{hyd}} = 25$–30% are found in the simulations; this is significantly more than for free ablation into vacuum. The reason for this is that the energy invested into the ablating, almost isothermal plasma is considerably reduced for tamped ablation because it cannot take up much kinetic energy. The high efficiency of capsule implosion is essential to compensate for the excessive losses of energy in the hotraum; only 15–20% of the absorbed beam energy is transfered to the fusion capsule, but with $\eta_{\mathrm{hyd}} = 30\%$ again a total coupling efficiency of $\eta_{\mathrm{c}} \simeq 5\%$ is obtained.

In conclusion, two alternative target options for heavy-ion beam fusion have been described, which imply different specifications for ion energy, ion current, beam focusing, and illumination geometry. Both types of targets are expected to have the potential for high gain when driven with 10 MJ pulses. The question which of them is the preferable one should be decided by considerations of accelerator and reactor design.

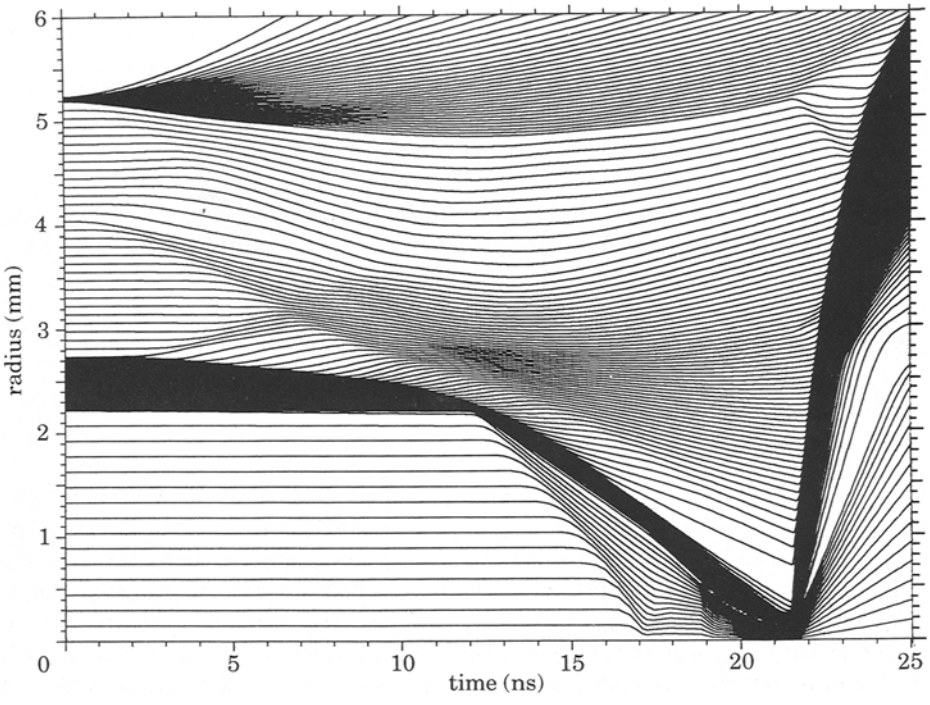

Fig. 5. – Hydrodynamics of hotraum target. Trajectories of Lagrangian cell interfaces are plotted in a radius-time diagram. In the shell of the fusion capsule and in the gold layer of the hotraum casing, the trajectories lie so dense that they appear as black areas. At early times, a shock is seen to run inwards, driven by the pressure in the deposition region. Simultaneously, capsule ablation drives a shock outwards. Both shocks collide at $t \simeq 6.5$ ns and $r \simeq 3.2$ mm. The ingoing shock then approaches the fusion capsule, but does not reach it due to strong radiatively driven ablation. At 12.3 ns, the first shock has passed the fuel capsule and is seen in the inner DT gas. The carbon layer is completely ablated, and the pusher-fuel shell is accelerated to about $2.5 \cdot 10^7$ cm/s. At 21.7 ns, the fuel ignites, and the expanding flow of the micro-explosion is observed.

4. – Tools for radiation hydrodynamics.

Concerning advanced future studies on indirect-drive targets for ion beam fusion, two types of computational tools are of particular importance:

– Codes for two-dimensional radiation hydrodynamics simulation of plasma configurations which are optically thick in some regions and optically thin in others. For studying radiative symmetrization, a condition is that deviations of the radiation field from an isotropic distribution, such as directed beams with sharp edges and corresponding shadows, are accurately described. Transport schemes based on the diffusion approximation are inadequate for this purpose.

– Numerical schemes for reliable calculation of group mean opacities, in particular for high-Z materials and mixtures of materials.

We have been working recently on both problems. Results are presented

in separate contributions to this conference. Here, we briefly discuss some general features of this work.

A new code (MULTI2D) for 2D radiation hydrodynamics has been developed in a cooperation between the Max-Planck-Institute for Quantum Optics at Garching and the Universidad Politecnica de Madrid [13]. The code describes hydrodynamics in two spatial dimensions and radiation transport along rays in three dimensions with the 4π solid angle discretized in 64 directions. Matter moves on a non-structured, triangular mesh. Radiation is transported according to a novel scheme; radiation flux of a given direction enters the triangular cells on two (one) sides of a triangle and leaves on the opposite side(s) in proportion to the viewing angles depending on the geometry. This scheme allows one to propagate sharply edged beams without ray tracing, though at the price of some lateral diffusion.

A new code (SAPHIR) has been developed for calculating emission and extinction coefficients of plasmas (including high-Z plasmas) over a wide range of temperatures and densities [14]. Detailed configuration account is used. The plasma state is calculated from a collisional-radiative model using stationary rate equations and including dielectronic recombination and excited configurations; it allows one to describe non-LTE situations. Concerning absorption coefficients, particular emphasis is put on line contributions; the atomic data are obtained from relativistic atomic structure calculations using parametrized potentials and accounting approximately for high-density effects. Presently, this work is extended to comprise mixtures of materials. Results will be used in future radiation hydrodynamics simulations.

REFERENCES

[1] J. LINDL, R. MCCRORY and E. M. CAMPBELL: *Phys. Today* (September 1992).
[2] J. MEYER-TER-VEHN: *Nucl. Fusion*, **22**, 561 (1982).
[3] S. ATZENI: *Part. Accel.*, **37**, 495 (1992).
[4] J. MEYER-TER-VEHN and M. MURAKAMI: *Part. Accel.*, **37**, 519 (1992).
[5] M. MURAKAMI and J. MEYER-TER-VEHN: *Nucl. Fusion*, **31**, 1315, 1333 (1991).
[6] M. BASKO and J. MEYER-TER-VEHN: *Nucl. Fusion*, **33**, 601 (1993).
[7] M. MURAKAMI, J. MEYER-TER-VEHN and R. RAMIS: *J. X-Ray Sci. Technol.*, **2**, 127 (1990).
[8] M. TEMPORAL and S. ATZENI: *Nucl. Fusion*, **32**, 557 (1992).
[9] K.-J. LUTZ, J. A. MARUHN and R. C. ARNOLD: *Nucl. Fusion*, **32**, 1609 (1992).
[10] G. BUCHWALD, G. GRAEBNER, J. THEIS, J. A. MARUHN, J. A. STÖCKER and H. KRUSE: *Laser Part. Beams*, **1**, 335 (1983).
[11] A. CARUSO and C. STRANGLIO: *Nucl. Fusion*, **31**, 1399 (1991).
[12] M. BASKO: *Nucl. Fusion*, **33**, 615 (1993).
[13] R. RAMIS and J. MEYER-TER-VEHN: MULTI2D—*A Computer Code for Two-Dimensional Radiation Hydrodynamics*, Max-Planck-Institut für Quantenoptik, Garching, Report MPQ174 (August 1992); this issue, p. 1907.
[14] A. RICKERT: *Zustand und optische Eigenschaften dichter Plasmen*, Max-Planck-Institut für Quantenoptik, Garching, Report MPQ175 (February 1993); A. RICKERT and J. MEYER-TER-VEHN: this issue, p. 1843.